Int. J. Heat Mass Transfer. Vol. 36, No. 16, pp. 3983–3996, 1993
Printed in Great Britain

0017–9310/93 $6.00+0.00

Single-phase thermosyphon cooling of an array of discrete heat sources in a rectangular cavity

M. S. POLENTINI, S. RAMADHYANI and F. P. INCROPERA
School of Mechanical Engineering, Purdue University, West Lafayette, IN 47907-1288, U.S.A.

(*Received* 1 *September* 1992 *and in final form* 30 *March* 1993)

Abstract—Experiments were performed with FC-77 and water to investigate free convection heat transfer from a 3×3 array of flush-mounted, discrete heat sources cooled by an opposing wall in a rectangular enclosure. The effects of the heater location, the enclosure width, the spacing between heaters, and the inclination of the enclosure were studied. For a vertical enclosure, heat transfer was a maximum and a minimum for the bottom and top rows of heated elements, respectively. Heat transfer was not affected by changes in the enclosure aspect ratio. On inclining the enclosure toward a horizontal (heated from below) orientation, the flow became unsteady and three-dimensional, resulting in significantly enhanced heat transfer for the upper element rows.

INTRODUCTION

HEAT TRANSFER considerations play an important role in the design of computer circuitry, since both the reliability and the speed of solid-state electronic devices decrease as their operating temperatures increase. Advances in integrated circuit technology have resulted in progressive increases in the number of electronic components that may be accommodated on a single chip. The higher component densities have been accompanied by progressively higher chip heat dissipation rates that are projected to exceed the limits of conventional thermal management approaches [1, 2]. Consequently, substantial efforts are being directed towards the development of advanced cooling techniques capable of meeting the needs of future high-density electronic packages. The present study is motivated by the projected cooling requirements of desktop computers, such as workstations and personal computers. While machines of this class currently are cooled by either free or forced convection of ambient air, it is believed that, in the future, cooling by direct immersion of the chips in a dielectric liquid may become necessary.

The simplest liquid-immersion scheme involves cooling by a passive single-phase thermosyphon arrangement in which the chips are mounted on one wall of a liquid-filled enclosure, while some of the other walls are externally cooled. The resulting temperature differences produce a circulating flow in the enclosure due to natural convection, and heat is transferred from the chips to the cooled walls. This scheme eliminates the need for a pump to sustain the flow, resulting in simple, quiet, cooling. Since the thermal expansion coefficients and Prandtl numbers of the fluorocarbon liquid coolants under consideration are high, Rayleigh numbers (based on chip length) as high as 10^8 may be achieved in such systems despite the small physical dimensions of the chips.

Several previous investigators have studied natural convective heat transfer from small, discrete, heat sources in an enclosure. Chu *et al.* [3] presented a numerical study of two-dimensional, laminar, natural convection from a long, horizontal, isothermal heated strip flush mounted on one vertical wall of an air-filled rectangular cavity. The opposing vertical wall was cooled, while the top and bottom walls were either adiabatic or cooled. The computations, involving parametric variations of the size and location of the heater, were restricted to low Rayleigh numbers, the highest value considered (based on cavity height) being 10^5. A similar configuration was studied experimentally by Turner and Flack [4] for higher Rayleigh numbers ranging up to 6×10^6. Kuhn and Oosthuizen [5] presented a numerical study of natural convection from a small, rectangular, chip-like, heating element located on one wall of a rectangular air-filled enclosure, the opposing wall being cooled. As in the study by Chu *et al.*, the effects of the size and location of the heating element were examined for low Rayleigh numbers. The applicability of the aforementioned studies to liquid immersion cooling of arrays of chips is limited, inasmuch as only single heat sources were considered, the coolant was air, and the studies were restricted to modest Rayleigh numbers.

Kelleher *et al.* [6] conducted an experimental study of natural convection from a single heated strip in a water-filled enclosure, the top and bottom walls of which were cooled. The study encompassed the range of Rayleigh numbers (based on strip height) between 10^6 and 10^7. Flow visualization photographs showed strong convective motion above the level of the heated strip but virtually quiescent fluid below the strip. The results of this study were supported by parallel numerical simulations by Lee *et al.* [7]. A recent numerical study by Wroblewski and Joshi [8] was focused on transient natural convection from a single chip package attached to one wall of a liquid-filled

NOMENCLATURE

A_h	surface area of a heated element
C_c	column heat loss correction factor
C_r	row heat loss correction factor
g	acceleration due to gravity
H	height of enclosure
$\bar{h}$	average heat transfer coefficient, $Q_c/A_h(T_h-T_c)$
k	thermal conductivity
L	length of a heated element
$\overline{Nu}_L$	average Nusselt number, $\bar{h}L/k$
$\overline{Nu}_y$	average Nusselt number, $\bar{h}y/k$
Nu_y	local Nusselt number, hy/k
Pr	Prandtl number
Q	power dissipation in the electric resistance heater
Q_c	corrected heat loss
Ra_L	Rayleigh number, $g\beta(T_h-T_c)L^3/(\nu\alpha)$
Ra_y	Rayleigh number, $g\beta(T_h-T_c)y^3/\nu\alpha$
Ra_y^*	modified Rayleigh number, $Nu_y Ra_y$
S	element spacing
T	temperature
W	width of enclosure (spacing between heated and cooled walls)
y	height of the center of each heated element from a given reference.

Greek symbols

α	thermal diffusivity
β	coefficient of thermal expansion
ν	kinematic viscosity
ϕ	angle of inclination.

Subscripts

c	cold wall
f	fluid
h	heated element.

enclosure. Water and the dielectric liquid FC-75 were employed as coolants, and conjugate heat transfer through the mounting wall was considered in the calculations.

In multi-chip arrays, thermal plumes arising from chips located at the bottom of the array might be expected to have an effect on chips located higher up. Chadwick *et al.* [9] presented a combined experimental and numerical study of two heated strips on a vertical wall of a rectangular enclosure. The opposing wall was cooled and the cavity was filled with air. The thermal plume rising from the lower heater was found to diminish the heat transfer coefficient at the upper heater by as much as 40%.

Carmona and Keyhani [10] conducted an experimental study of natural convection from five, vertically spaced, flush-mounted, heated strips in a tall cavity with the top wall cooled and all the other walls insulated. Ethylene glycol was used as the coolant. This study was later extended by Keyhani *et al.* [11] to include protruding heated strips. Thermal plume effects were evident in both studies, although the more complicated flow associated with the protruding strips resulted in a partial disruption of the plume and a less severe reduction of the heat transfer coefficient at the upper heaters. Unfortunately, the practical utility of the results presented in refs. [10, 11] is diminished by the fact that, in both studies, the surface area of the cooled wall was less than the combined surface areas of the heated strips. In both of these studies, the surface area of the cooled top wall was varied parametrically by varying the cavity width. Systematic increases in the effective heat transfer coefficients at the heated strips were observed with increases in the cavity width, indicating that the heat transfer from the strips was primarily limited by the relatively small area of the cooled wall.

An experimental study in which the large area of the opposing wall was used as the heat sink was reported by Keyhani *et al.* [12]. In this study, 11 flush-mounted, uniformly heated strips, spaced by unheated sections of the same width, were mounted in a tall ethylene glycol-filled enclosure with insulated top and bottom walls. The highest Rayleigh number (based on the strip width) achieved in their experiments was about 5×10^6. Flow visualization studies showed the existence of a large primary recirculating flow between the two vertical walls, as well as multiple smaller secondary eddies embedded within the primary loop. In general, heat transfer coefficients were found to diminish from the lowermost heater to the uppermost heater, although the decrease from heater to heater was not uniform. It was also found that Nusselt numbers, based on the height of each heater above the bottom of the enclosure, could be correlated against the modified Rayleigh numbers based on the same length scale, by a single equation applicable to all the heaters. This correlating equation was in close agreement with a standard correlation for a uniformly heated vertical plate in an infinite medium, suggesting that the heat transfer rates were controlled by the free convection boundary layers on the heated strips.

In an additional investigation, Prasad *et al.* [13] experimentally determined the effect of the width of the cavity on heat transfer from three uniformly heated strips with ethylene glycol as the coolant. In concurrent numerical simulations they examined the effect of the fluid Prandtl number. Heater Nusselt numbers were found to be virtually insensitive to variations in the cavity width (for $H/W \geqslant 3$) and to correlate with the Rayleigh number for $Pr \geqslant 1$. Both these findings are consistent with the dominance of the thermal resistances of the boundary layers on the heated strips. Prasad *et al.* chose to correlate the

heater Nusselt numbers against a Rayleigh number based on the total height of the cavity, thus necessitating separate correlating equations for each of the three heaters. Many of the results reported by Prasad *et al.* may also be found in refs. [14, 15].

A few studies of heat transfer from arrays of discrete square or rectangular heat sources have been reported. Liu *et al.* [16] presented a limited numerical study for a 3×3 array of equally-heated rectangular protrusions mounted on one wall of an enclosure filled with FC-75 and cooled from the top and bottom. The horizontal spacing between the sources was comparable to their longest dimension and the protrusion from the wall was sizable. Although the computations were restricted to low Rayleigh numbers, the computed flow patterns were found to be extremely complex, with substantial flow penetration into the gaps between adjacent heat sources. Experimental studies of similar configurations by Joshi *et al.* [17, 18] for Rayleigh numbers as high as 10^7 confirmed that the flow patterns were highly three-dimensional and time-dependent. In contrast to previously mentioned results for multiple flush-mounted strips, relatively small heater-to-heater variations in the Nusselt numbers were measured, indicating that the thermal plumes formed at the bottom heat sources were disrupted by the complex flow in the gaps between heaters.

The foregoing literature survey shows that the available information pertinent to liquid-immersion cooling of electronic chip arrays is limited. Although a sizable body of literature has been generated on natural convection from heated strips, and a few studies of protruding block-like heat sources in an enclosure have been reported, no previous results appear to have been published on natural convection from arrays of flat chip-like heat sources in an enclosure. While previous investigations indicate that complex three-dimensional flows occur with arrays of block-like heat sources, it is unclear whether such flows would occur with arrays of flush heaters. In addition, most of the previous work has been restricted to Rayleigh numbers lower than those associated with liquid-immersion cooling. Consequently, the available literature provides limited guidelines for the design of single-phase thermosyphon liquid-immersion cooling schemes for multi-chip arrays.

The objective of this paper is to report experimental data for an array of flush mounted heat sources on one vertical wall of a rectangular cavity, with the opposite wall cooled. Experiments have been performed over a wide range of Rayleigh numbers for a 3×3 array of 12.7 mm square heat sources using both water and dielectric liquid FC-77 (manufactured by 3M Co.) as coolants. Data have been taken to determine the effects of the heater location, the enclosure width, the spacing between heaters, and the boundary condition along the top wall of the cavity. In addition, while previous efforts have been focused exclusively on vertical cavities, the present paper includes information on the effect of inclining the cavity. The data are presented for individual heaters using dimensionless parameters.

EXPERIMENTAL METHODS

The experimental setup consisted of a test cell and a support structure that allowed for variation of the test cell orientation. The test cell, shown schematically in Fig. 1, consisted of a heater plate, an opposing cold plate, and a spacer plate/insert assembly compressed between two clamping plates by bolts passing through each corner. O-rings were used to seal the interfaces between the components. The heater plate was fabricated out of Lexan due to the strength and low thermal conductivity of this material. Two threaded holes were located near the top of the plate to allow for filling and draining of the test cell. These ports communicated with the test cell cavity through long slots machined in the surface of the plate. For the tests, a tube fitting was placed in each hole, and a length of polyethylene tubing, with the free end open to the atmosphere, was attached to each fitting, to allow for fluid expansion.

The heater plate supported a 3×3 array of 12.7 mm $\times$ 12.7 mm $\times$ 9.5 mm oxygen-free copper blocks arranged as shown in Fig. 2. Each block was instrumented with two copper–constantan thermocouples (0.127 mm wire diameter) located in holes drilled from the side 1.6 mm below the front surface of the block. The Lexan around each element was beveled, and a sealing compound was applied in the resulting groove at the Lexan/copper block interface. A thick-film resistive heater, composed of a 0.25 mm thick alumina

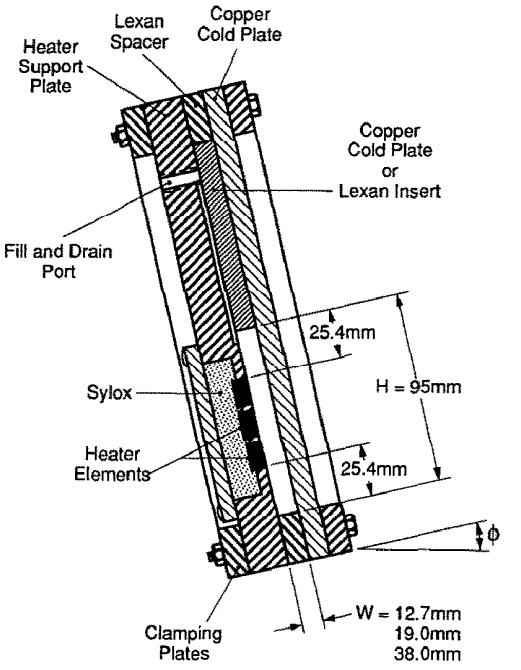

FIG. 1. Schematic depiction of the test cell.

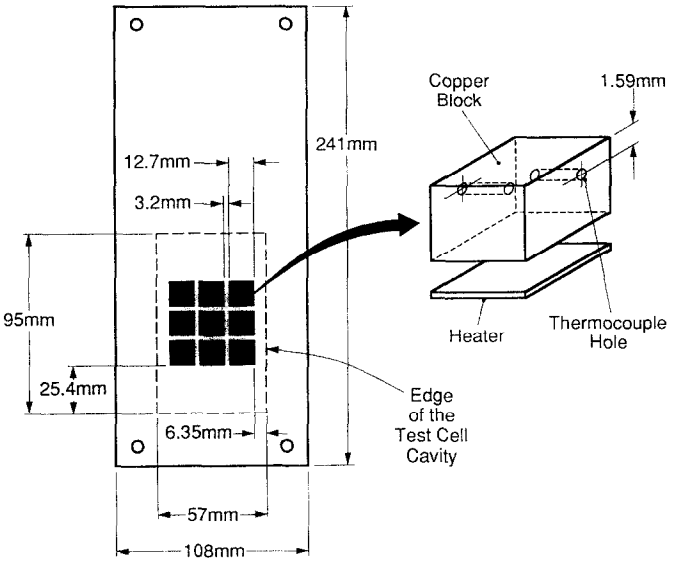

FIG. 2. Arrangement of the heat sources in the test cell cavity.

substrate with a 100 Ω resistive film, was soldered to the back of each block (see Fig. 2). The cavity behind the heaters was filled with an insulating material (Sylox, $k = 0.02$ W m^{-1} K^{-1}) to minimize heat losses through the back of the module.

The water-cooled cold plate opposite to the heaters was made of copper which, due to its large thermal conductivity, provided a near-uniform plate temperature. The plate contained an internal maze of channels through which water from a constant temperature bath could be circulated. The surface temperature of the cold plate was registered by three copper–constantan thermocouples soldered flush with the front surface.

A spacer plate/insert assembly was located between the heater plate and the cold plate. The frame-shaped Lexan spacer plate provided the side walls of the enclosure and controlled the spacing between the heater plate and cold plate. Spacers of three different thicknesses (12.7, 19 and 38.1 mm) were used during the course of the experiments. The transparency of the Lexan side walls allowed for optical access for flow visualization studies. An insert was attached inside the upper part of the plate to provide the top wall of the enclosure. The insert design varied depending on the test.

Two different inserts were used for the experiments. One insert was made of Lexan to provide a nearly adiabatic top boundary condition in the enclosure. The other insert was a cold plate made of copper. Like the enclosure side wall cold plate, the top cold plate contained cooling water channels. Two copper–constantan thermocouples were surface mounted to the exposed face of this cold plate.

When all the plates were assembled, the resulting cavity was 95 mm high and 57 mm deep. The spacing between sidewalls of the enclosure varied with the experiment. The elements in the heated wall of the enclosure were located 25.4 mm from the top and bottom enclosure walls and 6.35 mm from the side walls.

The experiments were conducted with FC-77 (manufactured by 3M Co.) and water. In order to eliminate the formation of air bubbles at the Lexan/copper interface when operating at high power inputs, each of these fluids were degassed before a given experiment. The test cell was filled with the degassed fluid, clamped to the mounting apparatus, and carefully leveled. The test cavity was either oriented vertically or inclined at a prescribed angle. The water supply to the cold plates was activated, and the power supplied to each heater was uniformly incremented. A D.C. power supply was used to energize the heaters. The temperatures and powers were scanned using a HP 3054 Data Acquisition System, and the temperature of the cooling water was monitored and adjusted to maintain desired cold plate temperatures.

Temperatures and power inputs were recorded when steady state was reached. Steady conditions were usually deemed to have been achieved when the temperature difference between any element and the cold plate did not vary by more than 0.05°C over a 5 min interval. At steady state, temperatures and power inputs were scanned 10 times during a 4 min interval and averaged.

As part of the experiments, flow visualization studies were performed for several test conditions. These studies, which were performed separately from the heat transfer measurements, included both the shadowgraph and particle tracing techniques. In the shadowgraph, a collimated beam of light from a mercury arc lamp was passed through the transparent Lexan side wall of the enclosure from behind and projected onto a piece of frosted glass placed on the

front of the test cell. Variations in the refractive index of the fluid due to density changes caused variations in brightness of the projected image and provided a qualitative impression of the flow pattern. In the particle tracing studies, the motion of small particles suspended in the liquid was used to infer flow patterns. Due to their near-neutral buoyancy in the respective fluids, finely ground fish scales were used with FC-77, and small diameter pliolite (specific gravity = 1.02) particles were used with water. A sheet of light from an argon laser was passed through the bottom wall of the test cell to illuminate a thin layer of particles in the fluid along a given column of heaters. Time-exposure photographs, with exposure times ranging from four to ten seconds, were taken to obtain particle streaks, which gave qualitative flow field information.

All of the tests were conducted under conditions of equal power dissipation (Q) for each of the heaters powered. All fluid properties were evaluated at a film temperature defined by

$$T_f = \frac{T_c + T_h}{2} \tag{1}$$

where T_c is the average of the three temperatures measured on the cold plate and T_h is the average of the two temperatures registered by the thermocouples of a given element. The two thermocouples on any given element agreed within 0.1°C in all cases. For tests involving two cold plates, both were maintained at the same nominal temperature, and T_c was defined as the average of the temperature readings on the two cold plates. For each element, the data were reduced in terms of Nusselt and Rayleigh numbers.

The Rayleigh number was defined as

$$Ra_L = \frac{g\beta(T_h - T_c)L^3}{\nu\alpha} \tag{2}$$

where the characteristic length, L, was the heater length. In some cases, another Rayleigh number was defined as

$$Ra_y = \frac{g\beta(T_h - T_c)y^3}{\nu\alpha} \tag{3}$$

y being the height of the center of each heater with respect to a given reference.

The Nusselt number was defined as

$$\overline{Nu_L} = \frac{\bar{h}L}{k} = \frac{Q_c L}{kA_h(T_h - T_c)} \tag{4}$$

where A_h is the surface area of the element. An alternative definition of the Nusselt number was used in some cases, with a characteristic length, y, defined as the height of an element above a given reference. The corrected heat loss, Q_c, was the heat transferred directly from the surface of the copper block to the fluid and was defined as

$$Q_c = QC_cC_r \tag{5}$$

Q being the measured power input to the given element. C_c and C_r were numerically determined substrate heat loss correction factors accounting for heat loss by a column of elements and a row of elements, respectively. The row loss correction factors ranged from 0.765 to 0.976, depending on the test and power input, while the values of C_c ranged from 0.850 to 0.970 and 0.888 to 0.976 for the side and center columns, respectively. The numerical simulations that resulted in these correction factors are described in detail by Polentini [19].

The maximum uncertainties associated with measured values of L and Q were 1 and 2%, respectively. All the thermocouples were calibrated to within 0.05°C of each other, and the maximum uncertainty associated with $(T_h - T_c)$ was 2%. The estimated uncertainties in the reported values of Nusselt number and Rayleigh number, as computed by the procedure described by Kline and McClintock [20], were 8 and 3%, respectively. The estimated uncertainty in the Nusselt number includes the uncertainty associated with the heat loss correction factors. In computing the foregoing uncertainty estimates, uncertainties in the fluid thermophysical properties were ignored. Therefore, the actual uncertainties (especially in the FC-77 data) are likely to be somewhat higher.

To facilitate the investigation of several of the parameters of interest, while minimizing the number of experiments performed, a set of standard conditions was defined. Parameters were then varied about these conditions. The standard condition tests were conducted with FC-77 in a vertical enclosure ($\phi = 0°$) of width $W = 12.7$ mm. The top wall of the cavity was adiabatic, and all the elements of the array were powered equally. The cold plate temperature was maintained at 25°C. To vary the Rayleigh number, the power input to each heater was varied from 0.3 to 1.9 W. Several additional experiments were performed by varying the power supplied to individual heater rows, the angle of inclination of the cavity, the cavity width, the fluid, and the top surface boundary condition. For tests with water, the heater power was varied from 0.3 to 7.0 W.

RESULTS

In discussing the results of the study, the standard conditions will be considered first to establish a reference for comparison. The heated elements will be represented by the following symbols unless otherwise specified: a circle for the top row elements, a triangle for the middle row elements, and a square for the bottom row elements. The flow patterns corresponding to some of the test conditions will be discussed in conjunction with the particle pathlines shown in Fig. 3. These pathlines were obtained by tracing over time-exposure photographs of the particle motion.

Standard conditions

The flow structure at standard conditions for a low heat input ($Q = 0.3$ W element^{-1}, $Ra_L \cong 10^7$) was

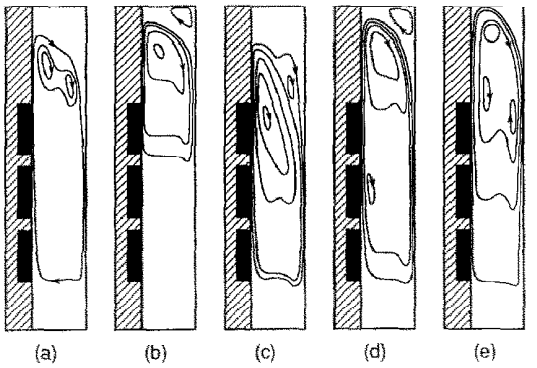

FIG. 3. Schematic rendering of particle pathlines for various test conditions: (a) standard conditions; (b) top row heated; (c) bottom row heated; (d) top and bottom rows heated; (e) water as the test fluid.

multicellular. A primary flow ascended along the heated wall and descended along the cold wall. As shown in Fig. 3(a), the primary cell enveloped two secondary cells, which rotated in the same direction and were located in the region above the top row of elements. Below the bottom row of elements, the fluid was relatively stagnant. The boundary layer remained laminar along the entire heated wall, and no significant columnwise variations in flow structure were observed. With increasing heat input, the boundary layer along the heated wall became turbulent above the top row of elements. While flow in the lower region of the enclosure did not significantly change from that observed at a low heat input, the unsteadiness of the flow in the upper region made it difficult to clearly delineate the particle tracks.

The foregoing flow structure differs from those numerically predicted by Keyhani *et al.* [14] and Shen *et al.* [15] for three isoflux elements. In those studies, which were performed for larger element spacings ($0.333 < S/L < 5$) and smaller Rayleigh numbers ($Ra_L < 3 \times 10^6$), multicellular flows were also predicted. However, the primary flow surrounded secondary flows that were located in regions between heated strips, in contrast to the observed secondary flows above the top row in the present case. This difference supports the conclusion drawn by Shen *et al.*, that the presence and location of secondary cells are dependent on the element spacing.

As expected, element temperatures were highest in the top row and lowest in the bottom row, clearly reflecting the effect of the growing thermal boundary layer on the upper element temperatures. Within each row, the temperatures of the center and side elements were in close agreement. A plot of $\overline{Nu}_L$ vs Ra_L for the standard condition is shown in Fig. 4. For each of the rows, $\overline{Nu}_L$ increases with Ra_L at a nearly constant slope. Even the top row at high Ra_L follows the same trend, which suggests that the turbulence and unsteadiness present above the top row did not significantly affect heat transfer. The maximum $\overline{Nu}_L$ values are associated with the bottom row, while

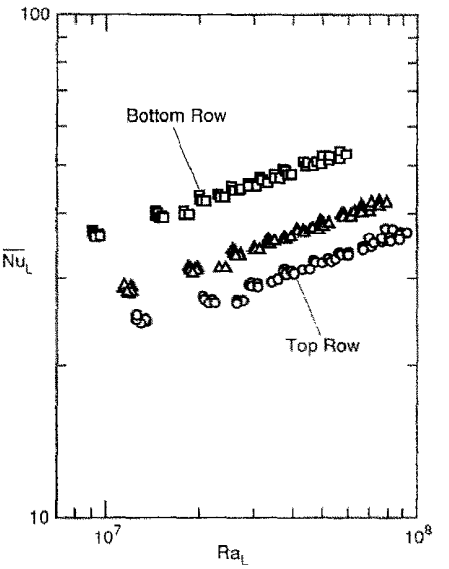

FIG. 4. Variations of the Nusselt numbers with Rayleigh numbers for the three rows under standard conditions (FC-77, $\phi = 0°$, $W = 12.7$ mm, $T_c = 25°$); circles: top row, triangles: middle row, squares: bottom row.

values for the middle row are about 22% smaller than those for the bottom row, and values for the top row are 32% smaller than those for the bottom row.

The data for each element row are correlated with a maximum deviation of 5% by the following equations:

$$\text{Top Row:}\quad \overline{Nu}_L = 0.767\, Ra_L^{0.211} \tag{6}$$

$$\text{Middle Row:}\quad \overline{Nu}_L = 0.849\, Ra_L^{0.215} \tag{7}$$

$$\text{Bottom Row:}\quad \overline{Nu}_L = 1.39\, Ra_L^{0.203}. \tag{8}$$

As shown in Fig. 5, the data for all of the elements

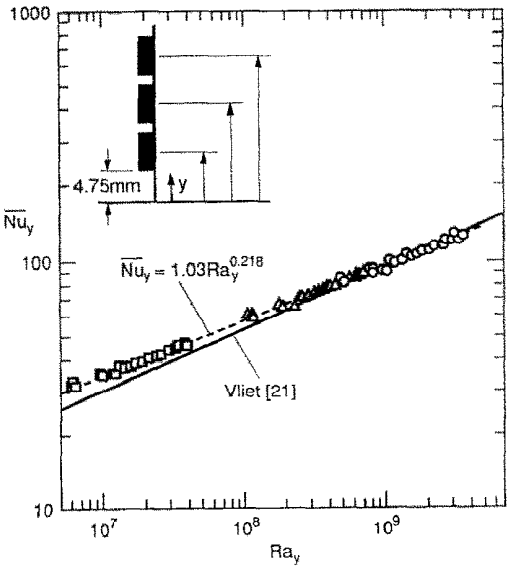

FIG. 5. Correlation of the Nusselt numbers for the three heater rows under standard conditions (FC-77, $\phi = 0°$, $W = 12.7$ mm, $T_c = 25°$).

are correlated by using a local length scale equal to the height of the center of a given element with respect to a location 4.75 mm below the bottom edge of the bottom row. The correlation, which shows a maximum deviation of 5%, is

$$\overline{Nu_y} = 1.03\, Ra_y^{0.218}. \quad (9)$$

Although an exact starting location for boundary layer development could not be determined, it was observed during the experiments that the boundary layer began to form slightly below the bottom row of elements, due to heat conduction into the substrate below the bottom row. Thus, the chosen reference location corresponds to a possible starting location of the boundary layer on the heated wall. It should be noted, however, that the starting location of the boundary layer depends on the ratio of the conductivities of the fluid and the substrate. Therefore, the correlation should be used with caution for different thermal conductivity ratios.

Vliet [21] developed a correlation for laminar natural convection heat transfer from an unconfined constant heat flux vertical wall:

$$Nu_y = 0.6\, Ra_y^{*0.2}. \quad (10)$$

The modified Rayleigh number, Ra_y^*, appearing in the correlation may be converted to the conventional Rayleigh number, Ra_y, through the relation $Ra_y^* = Nu_y Ra_y$. Substitution of this relationship into equation (10) results in

$$Nu_y = 0.528\, Ra_y^{0.25}. \quad (11)$$

The foregoing correlation is plotted on Fig. 5 for comparison with the data for the standard condition. At low Ra_y ($Ra_y = 10^7$), the data of this study exceed predictions based on the Vliet correlation for the continuously heated plate by as much as 18%. The difference decreases with increasing height (and Ra_y).

Figure 6 compares the standard condition data with correlations by Keyhani *et al.* [14] for three isoflux elements spaced one element width apart in an ethylene glycol ($105 < Pr < 166$) filled enclosure and Shen *et al.* [15] for $Pr = 25$ and a range of element spacings. Their correlations, which were given in terms of Ra_L^* and Ra_W^*, were expressed in terms of Ra_L to facilitate the comparison. Although the correlations presented in the previous studies cover lower ranges of Ra_L, it appears that, in general, values of $\overline{Nu_L}$ obtained in the current study exceed those of the previous studies if the correlations are extrapolated to higher Ra_L. The correlation by Keyhani *et al.* for the bottom row of elements is an exception. The higher Nusselt numbers in the current study may be attributed to three-dimensional effects at the side edges of the elements, which would enhance local convection at the edges [5].

Comparing the data at standard conditions to results obtained by Joshi *et al.* [17] for a 3×3 array of protruding sources in an enclosure cooled from the top and bottom for FC-75 ($Pr = 25$), it is apparent that the results of this study exceed values of $\overline{Nu_L}$ obtained using the correlation given by Joshi *et al.* The values of $\overline{Nu_L}$ calculated by Joshi *et al.* were based on the total wetted surface area of each protrusion, and the lower values may be due to lower heat transfer coefficients on the side surfaces of the protrusions.

Effect of heater location and spacing

To determine the effect of heater location, individual rows of elements were heated separately at heat inputs ranging from 0.3 to 1.6 W element^{-1} (Ra_L ranging from 1×10^7 to 5×10^7). For each case, the flow was relatively stagnant below the heated row and was steady and laminar for all heat inputs. Multicellular flows were observed for each case, with the secondary cells located in regions above the heated rows. Particle pathlines observed with only the top

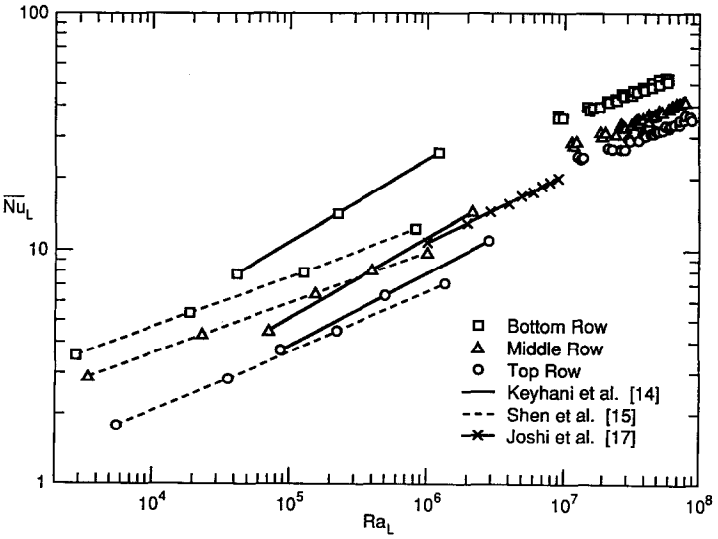

FIG. 6. Comparison of present data to the results of previous studies.

row heated and only the bottom row heated are presented in Figs. 3(b) and (c), respectively.

Heat transfer data for each of the rows heated individually showed no significant columnwise variation in $\overline{Nu_L}$. As expected, values of $\overline{Nu_L}$ for individually heated rows were larger than those for the standard case, since the effect of thermal plumes was eliminated. Although $\overline{Nu_L}$ did not differ significantly for the three heating conditions, values were highest and lowest for separate heating of the bottom and top rows, respectively. For the bottom row, values of $\overline{Nu_L}$ were 4–5% higher than for the middle row and 8–9% higher than for the top row.

An explanation for the increase in $\overline{Nu_L}$ with a decrease in element distance from the bottom of the enclosure is that the length of the primary flow cell increased, providing an increased distance of travel for the fluid along the surface of the cooled wall. This would result in the delivery of cooler fluid to the lower elements causing reduced temperatures in these elements. In the numerical study by Chu *et al.* [3] for a single heat source at a lower Pr and Ra_L, heat transfer was also found to increase with decreasing distance of the source from the bottom surface.

To determine the effect of spacing and location for two rows of elements heated simultaneously, combinations of rows were heated. When the bottom and middle rows and the top and middle rows of elements were heated, the flow below the lowest heated row was relatively stagnant, no major changes in flow structure were observed at higher heat inputs, and no turbulence was observed. There were no significant columnwise flow variations. Heating the top and bottom rows produced similar results. However, there appeared to be a secondary cell located near the middle row of elements. This structure, shown in Fig. 3(d), is similar to that predicted by Shen *et al.* [15], in which two secondary cells existed between heated elements. In the present case, however, an additional secondary cell was not clearly distinguished.

As shown in Fig. 7, heat transfer data for the various combinations of heated rows could be collapsed by using a length scale computed as the effective height of the center of a given row of elements with respect to a distance 6.4 mm below the bottom edge of the lowermost heated row. In computing the effective height, the space occupied by an unheated intermediate row was ignored, so that the same local height, y, was used for the top row when the top and bottom rows were heated as when the top and middle rows were heated. As can be seen from the graph, values of $\overline{Nu_y}$ do not deviate significantly for the three cases. However, slightly higher values of $\overline{Nu_y}$ can be seen for the case in which the top and bottom rows were heated. This behavior could be due to the presence of the secondary cell located between the elements in this case. This secondary cell could produce a partial dissipation of the thermal boundary layer between the bottom and top rows, leading to heat transfer enhancement. Compared to the case in which the middle and top rows were heated, a slightly higher $\overline{Nu_y}$ can be seen for the case in which the bottom and middle rows were heated, which could be due to the longer contact of the primary flow with the cold plate wall. Thus, for two rows of heat sources, $\overline{Nu_y}$ increases slightly with decreasing element distance from the bottom wall and increasing row spacing.

Effect of angle of inclination

In discussing the effects of inclining the enclosure, it should be noted that the component of gravity par-

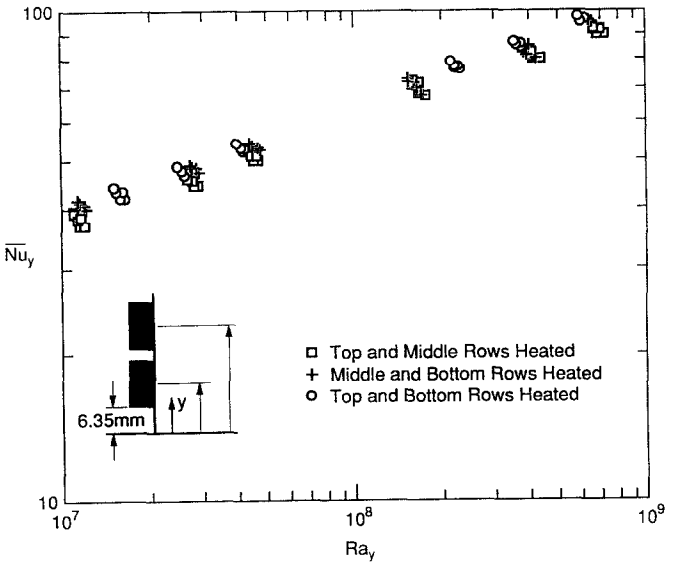

FIG. 7. Nusselt numbers for combinations of heated rows (FC-77, $\phi = 0°$, $W = 12.7$ mm, $T_c = 25°$).

allel to the element surfaces ($g\cos\phi$) was important for small angles of inclination, and the component normal to the element surfaces ($g\sin\phi$) became more important for angles of inclination approaching 90°. However, the Rayleigh number for the inclined enclosure was defined in the same way as for the standard case (i.e. based on g) to maintain a consistent definition.

For an inclination angle of 30°, shadowgraphs for a low heat input ($Q = 0.3$ W element^{-1}, $Ra_L \cong 10^7$) showed that the boundary layer became turbulent in the upper regions of the top row. Intermittent plumes of hot fluid were observed to ascend vertically from the boundary layer near the trailing edge of the top row. With an increase in heat input to 1.0 W element^{-1} ($Ra_L \cong 4\times10^7$), flow fluctuations in the upper part of the enclosure intensified. At higher heat inputs ($Q = 1.7$ W element^{-1}, $Ra_L \cong 7\times10^7$), plumes began to ascend from the surface near the middle row, and the region of turbulent fluctuations extended downward to the middle row of elements.

When the angle of inclination was adjusted to 45°, random, intermittent, turbulent plumes were again seen rising vertically from the top row and the upper region of the middle row of elements at a low heat input ($Q = 0.3$ W element^{-1}). Fluid in the region below the bottom edge of the bottom row was observed to be stagnant. As heat input was increased to 1.0 W element^{-1} ($Ra_L \cong 4\times10^7$), turbulent fluctuations intensified and moved downward in the enclosure, as buoyant plumes began to ascend from the entire surface of the middle row of elements. At heat inputs up to 1.7 W element^{-1} ($Ra_L \cong 7\times10^7$), the turbulence intensified in the region of the upper two rows of elements.

At an angle of inclination of 60°, turbulent fluctuations were again observed at the top and middle rows, and fluid below the bottom edge of the bottom row again appeared to be relatively stagnant. Unsteady plumes rising vertically from the elements caused heated fluid to impinge on the cold plate, ascend along the cold plate surface, and to circulate back down the heated wall toward the top row of elements. As the heat input was increased to 1.0 W element^{-1} ($Ra_L \cong 4\times10^7$), turbulent plumes were seen to rise from the bottom row.

At a 90° angle of inclination (heating from below), the flow approached the array of elements from the sides, was heated, and ascended towards the cold plate. The array appeared to act as a single source, due perhaps to the small spacing between elements. At a low power input ($Q = 0.3$ W element^{-1}, $Ra_L \cong 10^7$), the flow appeared to be slightly turbulent. When heat input was increased to 1.7 W element^{-1} ($Ra_L \cong 6\times10^7$), turbulent plumes rose from the entire array.

In general, for the 30, 45, and 60° inclinations, the Nusselt numbers at the bottom row of elements were highest. For the 30° inclination, the middle and top rows of elements had approximately equal $\overline{Nu_L}$ at the low heat inputs, with $\overline{Nu_L}$ for the top row becoming slightly larger at the higher Ra_L due to the action of the turbulence in the upper part of the enclosure. For the 45° inclination, values of $\overline{Nu_L}$ at the middle and top rows were approximately equal at low Ra_L. However, as Ra_L increased, $\overline{Nu_L}$ for the middle row approached that for the bottom row, while the top row had the lowest value. For the 60° inclination, row-to-row variations in $\overline{Nu_L}$ were relatively small. $\overline{Nu_L}$ was largest for the bottom and middle rows at low Rayleigh numbers, while at higher Ra_L the middle and top row values merged. For the 90° inclination, Nusselt numbers were found to be almost uniform on all the elements. The data for the four inclinations are correlated within a maximum deviation of 13% by the following equations:

$$\phi = 30°, \quad \overline{Nu_y} = 0.407\,Ra_y^{0.272} \tag{12}$$

$$\phi = 45°, \quad \overline{Nu_y} = 0.281\,Ra_y^{0.296} \tag{13}$$

$$\phi = 60°, \quad \overline{Nu_y} = 0.318\,Ra_y^{0.292} \tag{14}$$

$$\phi = 90°, \quad \overline{Nu_y} = 0.168\,Ra_y^{0.325} \tag{15}$$

where y is the same length scale used in the standard case ($y = 4.75$ mm). It should be noted that, although it is unconventional to use this length scale for a horizontal configuration, the correlation works well because the exponent on Ra_y is approximately equal to 1/3, thereby yielding results for which the convection coefficient is approximately independent of length scale. Figure 8 displays the data for the 45° inclination along with the correlating equation for that angle.

The data for the various inclinations are compared with those for the standard configuration by forming ratios of Nusselt numbers for the inclined configurations with the standard values. These ratios, which were obtained row by row, are displayed for the four inclinations in the four panels of Fig. 9. For $\phi = 30°$, there is significant enhancement relative to

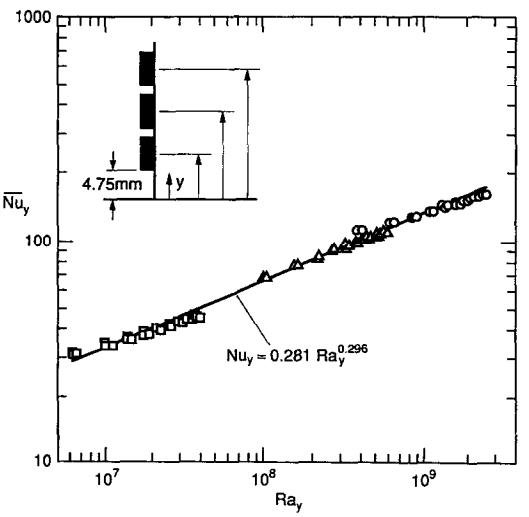

FIG. 8. Correlation of the data for $\phi = 45°$.

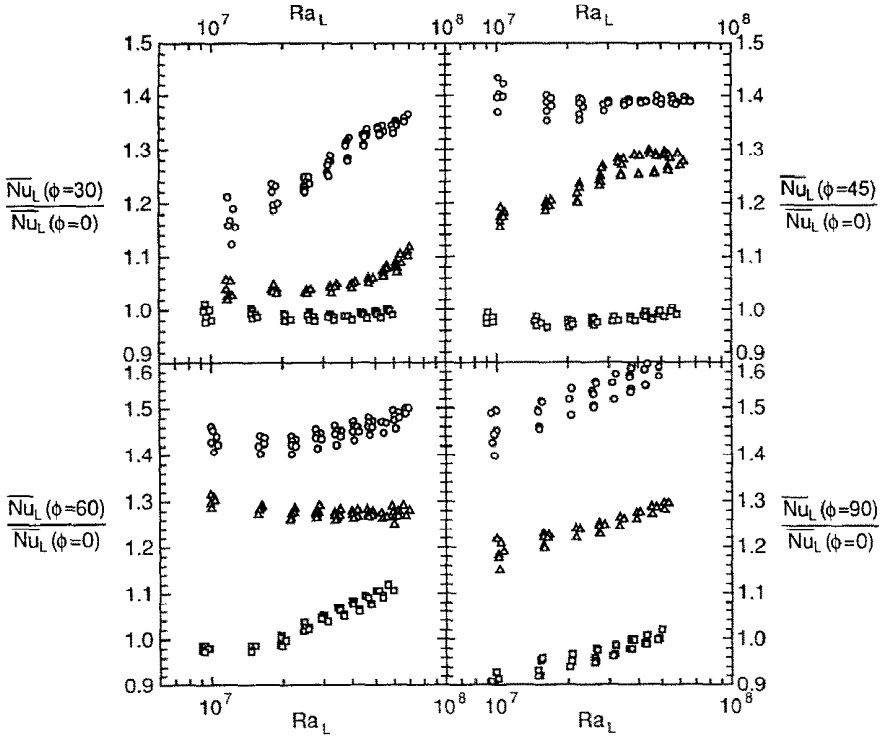

FIG. 9. Comparison of the Nusselt numbers for various angles of inclination with the standard condition values; circles: top row, triangles: middle row, squares: bottom row.

the standard case for the top row, and enhancement increases with increasing Ra_L. Although there is no enhancement for the bottom row, the middle row shows some enhancement which increases as Ra_L increases. The point at which significant enhancement occurs for the middle row corresponds to the heat input at which turbulence was observed near the middle row.

For $\phi = 45°$, the top row Nusselt number is greatly enhanced relative to the standard case (about 40%) while enhancement for the middle row increases with increasing Ra_L. Based on flow observations, this increase may be attributed to increased turbulence in the region occupied by the middle row. Values of $\overline{Nu}_L$ for the bottom row of elements are slightly smaller than values for the standard conditions. This result is attributed to a decrease in the gravitational acceleration component parallel to the element surfaces, which reduces velocity components parallel to the surfaces.

For $\phi = 60°$, both the middle and top row Nusselt numbers are greatly enhanced relative to the standard condition. $\overline{Nu}_L$ for the bottom row increases significantly with respect to the standard condition results at Ra_L corresponding to the inception of turbulence in the lower region of the enclosure ($Q = 0.7$ W element^{-1}, $Ra_L = 2 \times 10^7$). As in the 30 and 45 cases, the observations suggest that when significant enhancement occurs, it is due to turbulence in fluid motion adjoining the elements.

For $\phi = 90°$, the top row shows an enhancement that increases with Ra_L up to 60%, while the middle row displays an enhancement increasing with Ra_L up to 25%. The bottom row actually shows a decrease in $\overline{Nu}_L$ at low Ra_L compared to standard conditions and approaches the same $\overline{Nu}_L$ at high Ra_L.

To summarize the results of inclining the test cell with respect to the vertical, heat transfer increases with increasing angle of inclination. This trend is largely due to the onset and amplification of turbulence which propagates down the heated wall with increasing angle of inclination. For $\phi = 90°$, almost uniform cooling is obtained at all the elements.

Effect of vertical wall spacing (aspect ratio)

Although no particle traces were obtained for experiments in which the enclosure wall spacing was varied, shadowgraphs revealed results similar to those obtained at standard conditions. At a low heat input, the boundary layer was laminar, and fluid circulation in the enclosure was similar to that observed at standard conditions. At higher heat inputs, the boundary layer became turbulent above the top row of elements. The temperature and heat transfer data were nearly identical to data at standard conditions. There was very little change in $\overline{Nu}_L$ with enclosure width for the three widths studied. This result is consistent with previous studies by Shen *et al.* [15], which revealed no significant change in $\overline{Nu}_L$ with variation in the enclosure aspect ratio.

Effect of Prandtl number

In order to determine the effect of the Prandtl number of the fluid, experiments were performed using water ($Pr = 5$) instead of FC-77 ($Pr = 25$), with heat inputs ranging from 0.3 W element^{-1} ($Ra_L \cong 10^4$) to 7 W element^{-1} ($6 \times 10^5 \leqslant Ra_L \leqslant 3 \times 10^6$). Since water is a better coolant than FC-77, it was possible to operate at much higher heat inputs while maintaining heater temperatures within acceptable limits.

Flow visualization at a low heat input ($Q = 0.7$ W element^{-1}, $3 \times 10^4 \leqslant Ra_L \leqslant 4 \times 10^4$) revealed that, as in the standard case, fluid below the bottom row of elements remained relatively stagnant, the boundary layer remained laminar, and the flow structure, which was steady, did not vary significantly in the spanwise direction. As in the standard case, multicellular flows were observed. However, instead of the two secondary flow cells, which were observed for the standard case, three secondary cells were located at the top of the enclosure. With increases in heat input to 1, 4, and 7 W element^{-1} (Ra_L increasing to 3×10^6), there was no noticeable change in flow structure, and the boundary layer remained laminar while the flow remained steady. Figure 3(e) depicts the flow structure at a heat input of 4 W element^{-1} ($Ra_L \approx 10^5$).

As in the standard case, there were no significant differences in $\overline{Nu_L}$ for elements in a given row. The highest and lowest Nusselt numbers occurred for the bottom and top rows, respectively, as shown in Fig. 10. $\overline{Nu_L}$ increased with Ra_L at a constant slope for all rows. The data for FC-77 are included on the plot for comparison. If the trends exhibited by the water data are extrapolated into the range of the FC-77 data, differences of up to 15% are observed, the FC-77 data displaying the larger Nusselt numbers. Thus, it appears that the effect of the Prandtl number on the Nusselt number is modest. This supports the numerical and experimental results of Prasad *et al.* [13] which showed that, for an equivalent Rayleigh number, values of $\overline{Nu_L}$ for $Pr = 25$ and 166 were only 5% higher than $\overline{Nu_L}$ for $Pr = 1$.

All of the data for the experiments with water and FC-77 are correlated by row according to the following relations:

$$\text{Top Row: } \overline{Nu_L} = 0.242\, Ra_L^{0.276} \tag{16}$$

$$\text{Middle Row: } \overline{Nu_L} = 0.308\, Ra_L^{0.272} \tag{17}$$

$$\text{Bottom Row: } \overline{Nu_L} = 0.440\, Ra_L^{0.270}. \tag{18}$$

The maximum deviation from these correlations is 10% while most of the data is correlated to within 5%. As shown in Fig. 11, the data for FC-77 and water can be correlated by using a length scale equal to the local height of a given element with respect to a location 4.75 mm below the bottom edge of the bottom row according to the following correlation:

$$\overline{Nu_y} = 0.607\, Ra_y^{0.243}. \tag{19}$$

A maximum deviation of 20% and a standard deviation of 8% is associated with this correlation.

Effect of cooling top surface

To investigate the effect of adding additional cooling to the top surface of the enclosure, experiments were performed with a top cold plate, which was held at 25°C, for heat inputs ranging from 0.3 W element^{-1} ($Ra_L \cong 10^7$) to 1.9 W element^{-1} ($6 \times 10^7 \leqslant Ra_L \leqslant 9 \times 10^7$). FC-77 was used as the coolant. Flow visualization for these experiments revealed little change in the flow field compared to the standard

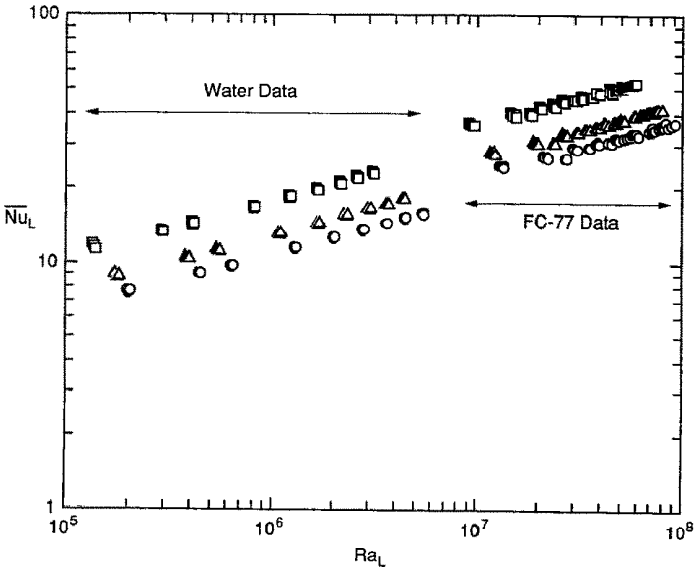

FIG. 10. Variations of the Nusselt numbers with Rayleigh numbers for the three rows with both water and FC-77 as test fluids; circles: top row, triangles: middle row, squares: bottom row.

condition case. The same multicellular flows were observed at low heat inputs, and the boundary layer along the heated wall became turbulent above the top row of elements with increasing heat input.

The heat transfer results differ from the standard condition case only slightly. As in the standard case, there was little difference in $\overline{Nu}_L$ for elements within a row. Nusselt numbers were largest for the bottom row and smallest for the top row. However, compared to the standard case, there is a slight enhancement in heat transfer for the top and middle rows of elements. Figure 12 shows that there is a 10% increase in $\overline{Nu}_L$ for the top row, and that enhancement increases only slightly with Ra_L. For the middle row of elements, there is a 5% enhancement relative to the standard conditions, while for the bottom row, there is very little change in $\overline{Nu}_L$. Values of $\overline{Nu}_L$ for the middle row of elements are approximately 81% of those for the bottom row, while values for the top row of elements are approximately 72% of those for the bottom row. The data for all three rows are correlated well using the relation

$$\overline{Nu}_y = 0.502\, Ra_y^{0.255} \qquad (20)$$

where the characteristic length, y, is the same as in the standard case.

CONCLUSIONS

Experimental data have been obtained for single phase thermosyphon cooling of a 3×3 array of small, square, flat heat sources. The experiments were performed with FC-77 ($Pr = 25$) for $10^7 < Ra_L < 10^8$, $2.5 \leqslant H/W \leqslant 7.5$ and $0 \leqslant \phi \leqslant 90^\circ$, as well as with water ($Pr = 5$) for $\phi = 0^\circ$ and $10^4 < Ra_L < 5 \times 10^6$. The following conclusions were drawn from the study:

1. In general, there were no spanwise variations in flow structure or heat transfer for the range of conditions considered.
2. For the standard case (FC-77, $\phi = 0^\circ$, $W = 12.7$ mm, $q_{top} = 0$), steady secondary flows were observed above the top row of elements in the enclosure at low Ra_L, and the boundary layer along the heated wall became turbulent above the top row with increasing Ra_L. The maximum and minimum $\overline{Nu}_L$ corresponded to the bottom and top row, respectively. It was possible to correlate the Nusselt numbers for the three rows against the Rayleigh number with a single equation (equation (9)) by using a characteristic length equal to the height of the center of a given element row above a reference location corresponding to the possible origin of the boundary layer. Values of $\overline{Nu}_L$ were slightly larger than those for a continuously heated plate in an infinite medium and discretely heated strip elements in an enclosure.
3. Values of $\overline{Nu}_L$ for individually heated rows were larger than those for the standard condition case. Although $\overline{Nu}_L$ did not differ significantly for each case, values were the highest and lowest for the bottom row heated alone and the top row heated alone, respectively. Values for bottom row heating were 4–5% higher than those for the middle row and 8–9% higher than those for the top row.
4. Data for two rows of simultaneously heated elements showed that values of $\overline{Nu}_L$ increased slightly with decreasing element distance from the bottom wall and increasing row spacing.
5. Increasing the angle of inclination increased

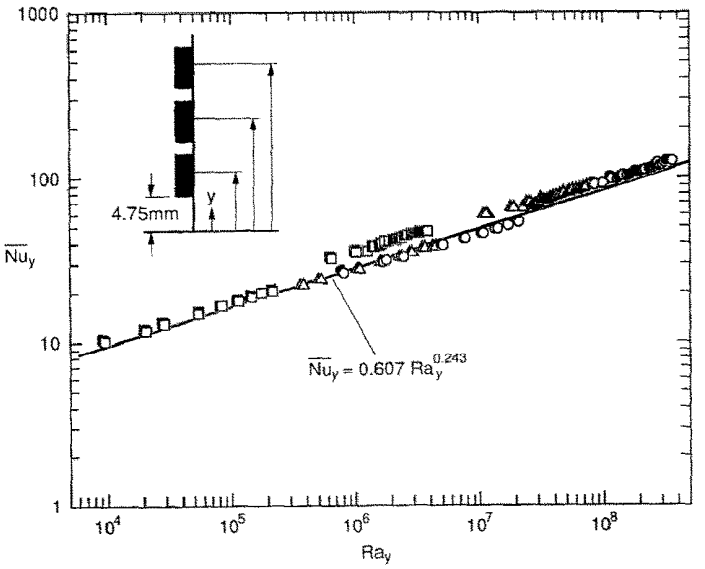

FIG. 11. Correlation of the water and FC-77 data ($\phi = 0^\circ$, $W = 12.7$ mm, $T_c = 25^\circ$).

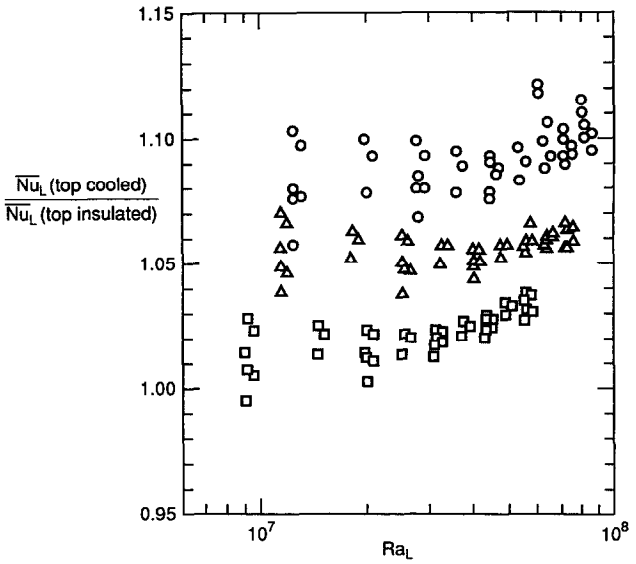

FIG. 12. Comparison of the Nusselt numbers for top surface cooling with the standard condition values (FC-77, $W = 12.7$ mm, $T_c = T_{top} = 25°C$).

values of $\overline{Nu_L}$ for the upper rows of elements. This enhancement, caused by the action of turbulent plumes, moved to the lower rows as the inclination angle and Ra_L increased. At an inclination of 90°, all of the elements of the array were cooled almost uniformly. The data for the four inclination angles were correlated by equations (12)–(15).

6. Varying the spacing between the vertical walls had no significant effect on $\overline{Nu_L}$ for the range of spacings studied.

7. It was possible to collapse the data for water ($Pr = 5$) and FC-77 ($Pr = 25$), by correlating the Nusselt number against the Rayleigh number. The data for water and FC-77 were correlated by a single equation (equation (19)) with a standard deviation of 6%.

8. Cooling the top surface of the enclosure in addition to the side surface produced no change in flow structure and resulted in only slightly different heat transfer results. Top surface cooling resulted in a 10% increase in $\overline{Nu_L}$ for the top row and a 5% increase for the middle row. No enhancement was seen for the bottom row.

Acknowledgement—This research was supported by the National Science Foundation under grant No. CTS-9004213.

REFERENCES

1. F. P. Incropera, Convection heat transfer in electronic equipment cooling, *J. Heat Transfer* **110,** 1097–1111 (1988).
2. A. Bar-Cohen, Thermal management of electronic components with dielectric liquids, *Proceedings of the ASME/JSME Thermal Engineering Joint Conference*, Vol. 2, XV–XXXIX (1991).
3. H.H.-S. Chu, S. W. Churchill and C. V. S. Patterson, The effect of heater size, location, aspect ratio, and boundary conditions on two-dimensional, laminar, natural convection in rectangular channels, *J. Heat Transfer* **98,** 194–201 (1976).
4. B. L. Turner and R. D. Flack, The experimental measurement of natural convective heat transfer in rectangular enclosures with concentrated energy sources, *J. Heat Transfer* **102,** 236–241 (1980).
5. D. Kuhn and P. H. Oosthuizen, Three-dimensional transient natural convective flow in a rectangular enclosure with localized heating, *Natural Convection in Enclosures*—1986, *ASME HTD*-63, pp. 55–62 (1986).
6. M. D. Kelleher, R. H. Knock and K. T. Yang, Laminar natural convection in a rectangular enclosure due to a heated protrusion on one vertical wall—part I: experimental investigation, *Proceedings of the ASME/JSME Thermal Engineering Joint Conference*, Vol. 2, pp. 169–178 (1987).
7. J. J. Lee, K. V. Liu, K. T. Yang and M. D. Kelleher, Laminar natural convection in a rectangular enclosure due to a heated protrusion on one vertical wall—Part II: numerical simulations, *Proceedings of the ASME/JSME Thermal Engineering Joint Conference*, Vol. 2, pp. 179–185 (1987).
8. D. Wroblewski and Y. Joshi, Transient natural convection from a leadless chip carrier in a liquid filled enclosure: a numerical study, *Proceedings of the ASME/JSME Joint Conference on Electronic Packaging*, EEP-Vol. 1-1, pp. 235–248 (1992).
9. M. L. Chadwick, B. W. Webb and H. S. Heaton, Natural convection from two-dimensional discrete heat sources in a rectangular enclosure, *Int. J. Heat Mass Transfer* **34,** 1679–1693 (1991).
10. A Carmona and M. Keyhani, The cavity width effect on immersion cooling of discrete flush-heaters on one vertical wall of an enclosure cooled from the top, *J. Electronic Packaging* **111,** 268–276 (1989).
11. M. Keyhani, L. Chen and D. R. Pitts, The aspect ratio effect on natural convection in an enclosure with protruding heat sources, *J. Heat Transfer* **113,** 883–891 (1991).
12. M. Keyhani, V. Prasad and R. Cox, An experimental study of natural convection in a vertical cavity with discrete heat sources, *J. Heat Transfer* **110,** 616–624 (1988).
13. V. Prasad, M. Keyhani and R. Shen, Free convection in a discretely heated vertical enclosure: effects of Prandtl

number and cavity size, *J. Electronic Packaging* **112,** 63–74 (1990).
14. M. Keyhani, V. Prasad, R. Shen and T.-T. Wong, Free convection heat transfer from discrete heat sources in a vertical cavity, *Natural and Mixed Convection in Electronic Equipment Cooling* (Edited by R. A. Wirtz), *ASME HTD*-100, pp. 12–24 (1988).
15. R. Shen, V. Prasad and M. Keyhani, Effect of aspect ratio and size of heat source on free convection in a discretely heated vertical cavity, *Numerical Simulation of Convection in Electronic Equipment Cooling* (Edited by A. Ortega and D. Agonafer), *ASME HTD*-121, pp. 45–54 (1989).
16. K. V. Liu, K. T. Yang and M. D. Kelleher, Three-dimensional natural convection cooling of an array of heated protrusions in an enclosure filled with a dielectric fluid, *Cooling Technology for Electronic Equipment*, p. 486. Hemisphere, New York (1988).
17. Y. Joshi, M. D. Kelleher and T. J. Benedict, Natural convection immersion cooling of an array of simulated electronic components in an enclosure filled with dielectric liquid. *Heat Transfer in Electronic and Microelectronic Equipment*, p. 445. Hemisphere, New York (1990).
18. Y. Joshi, M. D. Kelleher, M. Powell and E. I. Torres, Natural convection heat transfer from an array of rectangular protrusions in an enclosure filled with dielectric liquid, *Heat Transfer Enhancement in Electronics Cooling*, *ASME HTD*-183, pp. 9–18 (1991).
19. M. S. Polentini, Single and two-phase thermosyphon cooling of an array of discrete heat sources in a rectangular cavity, M.S.M.E. Thesis, Purdue University (1991).
20. S. J. Kline and F. A. McClintock, Describing uncertainties in single-sample experiments, *Mech. Engng* **75,** 3–8 (1953).
21. G. C. Vliet, Natural convection local heat transfer on constant-heat-flux inclined surfaces, *J. Heat Transfer* **91,** 511–516 (1969).